Broadband loss-less optical thin-film depolarizing devices

Quentin Ailloud, Myriam Zerrad, Claude Amra

Research Article | Vol. 26, No. 10 | 14 May 2018 | OPTICS EXPRESS 13264
Optics EXPRESS

Broadband loss-less optical thin-film depolarizing devices

QUENTIN AILLOUD,[1,2,*] MYRIAM ZERRAD,[1] AND CLAUDE AMRA[1,3]

[1] *Aix Marseille Univ, CNRS, Centrale Marseille, Institut Fresnel, Marseille, France*
[2] *CNES, 18 Avenue Edouard Belin, 31401 Toulouse Cedex 9, France*
[3] *CNRS, Ecole Centrale Marseille Institut Fresnel UMR 7249, 13013 Marseille, France*
[*] *quentin.ailloud@fresnel.fr*

Abstract: For some space applications, sensors are sensitive to light polarization and can only be properly calibrated with non-polarized light. Here we propose new optical devices which allow to depolarize light in a spatial process. These devices are thin film multilayers which exhibit polarimetric phase variations in their plane. A zero spatial polarization degree can be reached with high accuracy in a controlled bandwidth.

OCIS codes: (310.5448) Polarization, other optical properties; (260.2130) Ellipsometry and polarimetry.

References and links

1. C. Brosseau, *Fundamentals of Polarized Light: A Statistical Optics Approach* (Wiley, 1998).
2. F. Goudail and A. Bénière, "Estimation precision of the degree of linear polarization and of the angle of polarization in the presence of different sources of noise," Appl. Opt. **49**, 683–693 (2010).
3. L. Pouget, J. Fade, C. Hamelsection, and M. Alouini, "Polarimetric imaging beyond the speckle grain scale," Appl. Opt. **51** 7345–7356 (2012).
4. S. Ainouz, J. Zallat, A. Martino and C. Collet, "Physical interpretation of polarization-encoded images by color preview," Opt. Express **14**, 5916–5927 (2006).
5. L. Arnaud, G. Georges, J. Sorrentini, M. Zerrad, C. Deumié, and C. Amra, "An enhanced contrast to detect bulk objects under arbitrary rough surfaces," Opt. Express **17**, 5758–5773 (2009).
6. P. Elies, B. Le Jeune, P.Y. Gerligand, J. Cariou and Lotrian, "Analysis of the dispersion of speckle polarization on the Poincaré sphere," Appl. Phys. **30** 1285–1292 (1997).
7. P. Réfrégier, J. Fade, and M. Roche, "Estimation precision of the degree of polarization from a single speckle intensity image," Opt. Lett. **32**, 739–741 (2007). section
8. M. Born and E. Wolf, *Principles of Optics* (Pergamon Press, 1970).
9. M. Zerrad, C. Luitot, J. Berthon, and C. Amra, "Optical systems for controlled specular depolarization," Opt. Lett. **39**, 6919–6922 (2014).
10. E. Collett, *Field Guide to Polarization* (SPIE, 2005).
11. M. Zerrad, C. Amra, "Dépolariseurs spéculaires parfaits," patent FR1454923 (2014).
12. A. Ghabbach, M. Zerrad, G. Soriano, S. Liukaityte, and C. Amra, "Depolarization and enpolarization DOP histograms measured for surface and bulk speckle patterns," Opt. Express **22**, 21427–21440 (2014).
13. B. Liu, M. Harman, and M. E. Brezinski, "Variables affecting polarization-sensitive optical coherence tomography imaging examined through the modeling of birefringent phantoms," J. Opt. Soc. Am. A **22**, 262–271 (2005).
14. M. Zerrad, J. Sorrentini, G. Soriano, and C. Amra, "Gradual loss of polarization in light scattered from rough surfaces: electromagnetic prediction," Opt. Express **18**, 15832–15843 (2010).
15. Jan Dupont and Xavier Orlik, "Simulation of polarized optical speckle fields: effects of the observation scale on polarimetry," Opt. Express **24**, 11151–11163 (2016).
16. J. Sorrentini, M. Zerrad, and C. Amra, "Statistical signatures of random media and their correlation to polarization properties," Opt. Lett. **34**, 2429–2431 (2009).
17. J. Sorrentini, M. Zerrad, G. Soriano, and C. Amra, "Enpolarization of light by scattering media," Opt. Express **19**, 21313–21320 (2011).
18. A. Ghabbach, M. Zerrad, G. Soriano, and C. Amra, "Accurate metrology of polarization curves measured at the speckle size of visible light scattering," Opt. Express **22**, 14594–14609 (2014).
19. M. Zerrad, A. Ghabbach, G. Soriano, M. Lequime, C. Amra, and J. Berthon, "Depolarizing optical multilayers," in Optical Interference Coatings, M. Tilsch and D. Ristau, ed. (OSA Technical Digest, 2013).
20. R. M.E. Illing, "Optical and structural performance of the PolZero-Lm time domain polarization scrambler," presented at the Earth Science Technology Forum, Boulder, USA, 22 Jun. 2010.
21. J. Caron, J.L. Bézy, G. Bazalgette Courrèges-Lacoste, B. Sierk, R. Meynart, M. Richert, D. Loiseaux, "Polarization scramblers in Earth observing spectrometers: lessons learned from Sentinel-4 and 5 phases A/B1," presented at the International Conference on Space Optics - ICSO, Ajaccio, France, 9-12 Oct. 2012.

#324823 https://doi.org/10.1364/OE.26.013264
Journal © 2018 Received 28 Feb 2018; revised 4 Apr 2018; accepted 5 Apr 2018; published 8 May 2018

Optics EXPRESS

22. L. Abel-Tibérini, F. Lemarquis, and M. Lequime, "Masking mechanisms applied to thin-film coatings for the manufacturing of linear variable filters for two-dimensional array detectors," Appl. Opt. **47**, 5706–5714 (2008).
23. J. Broky and A. Dogariu, "Correlations of polarization in random electro-magnetic fields," Opt. Express **19**, 15711–15719 (2011).
24. A. V. Tikhonravov, P. W. Baumeister, and K. V. Popov, "Phase properties of multilayers," Appl. Opt. **36**, 4382–4392 (1997).
25. J. D. T. Kruschwitz, V. Pervak, J. Keck, I. Bolshakov, Z. Gerig, F. Lemarchand, K. Sato, W. Southwell, M. Sugiura, M. Trubetskov, and W. Yuan, "Optical interference coating design contest 2016: a dispersive mirror and coating uniformity challenge," Appl. Opt. **56**, C151–C162 (2017).
26. E. N. Kotlikov, V. N. Prokashev, V. A. Ivanov, and A. N. Tropin, "Thickness uniformity of films deposited on rotating substrates," J. Opt. Technol. **76**, 100–103 (2009).
27. M. Lequime and C. Amra. *De l'Optique électromagnétique à l'Interférométrie - Concepts et illustrations* (EDP Sciences, 2013).
28. J. W. Goodman, *Introduction to Fourier Optics* (Roberts and Company Publishers, 1996).
29. MacLeod (H.A.) et MacLeod (A.), *Thin Film Optical Filters* (Taylor and Francis, 2001).
30. Baumeister(P.W.), *Optical Coating Technology* (SPIE Press Book, 2004).
31. A. V. Tikhonravov, "Some theoretical aspects of thin-film optics and their applications," Appl. Opt. **32**, 5417–5426 (1993).
32. M. Bass, *Handbook of Optics: Volume IV - Optical Properties of Materials, Nonlinear Optics, Quantum Optics*, (McGraw Hill Professional, 2010) Chap. Optical Properties of Films and Coatings.
33. M. Gross, S. Dligatch, and A. Chtanov, "Optimization of coating uniformity in an ion beam sputtering system using a modified planetary rotation method," Appl. Opt. **50**, C316–C320 (2011).
34. L. Abel-Tiberini, F. Lemarquis, and M. Lequime, "Dedicated spectrophotometer for localized transmittance and reflectance measurements," Appl. Opt. **45**, 1386–1391 (2006).
35. W. D. Shen, M. Cathelinaud, M. Lequime, F. Charpentier, and V. Nazabal, "Light trimming of a narrow bandpass filter based on a photosensitive chalcogenide spacer," Opt. Express **16**, 373–383 (2008).
36. F.D. Ismail, M. Aziz, C. Teeka, J. Ali, and P. Yupapin, "Filter design using multi-Bragg reflectors," World Journal of Modelling and Simulation **8**, 205-210 (2012).
37. M. Zerrad, H. Tortel, G. Soriano, A. Ghabbach, and C. Amra, "Spatial depolarization of light from the bulks: electromagnetic prediction," Opt. Express **23**, 8246–8260 (2015).
38. M. Gorman, and S.A. Solin, "Transmission Raman and depolarization spectra of bulk a-Se from 13 to 300 cm^1," Solid State Commun. **18**, 0038–1098 (1976).
39. N. J. Diorio Jr., M. R. Fisch, and J. L. West, "Filled liquid crystal depolarizers," J. Appl. Phys. **90**(8), 3675–3678 (2001).
40. W. Domañski, "Polarization degree fading during propagation of partially coherent light through retarder," Opto-Electron. Rev. **13** (2005).
41. O. Polat, Y. Emül, and S. Özharar, "Investigation of the Mueller Matrix elements of the liquid crystal cell illuminated with a broad band light source," in *Optical and Quantum Electronics* (Springer, 2017).
42. O. Polat, "Theoretical study on depolarization of the light transmitted through a non-uniform liquid crystal cell," Optik **7**, 3560–3563 (2016).
43. A. Ghabbach, M. Zerrad, G. Soriano, S. Liukaityte, and C. Amra, "Depolarization and enpolarization DOP histograms measured for surface and bulk speckle patterns," Opt. Express **22**, 21427–21440 (2014).

1. Introduction

Polarized light is usually considered to be an added value and is often used to improve the observation of samples and scenes, due to optimization processes [1–12] . However there is a number of situations where this light property must be cancelled, that is, where polarized light (dop = 1) must be turned into unpolarized light (dop = 0), with dop the polarization degree. As an illustration, specific space applications require light to be fully depolarized with high accuracy, so as to calibrate optical systems or devices that are polarization sensitive.

Although one can easily transform the polarization state of light into another arbitrary state (both with dop = 1), the converse situation is less common and is often accompanied by optical losses and a reduction of spatial or temporal coherence [13–19]. Hence different kinds of devices and systems were designed and built to reach this depolarization function, on the basis of [20, 21].

In this paper we propose an alternative technique based on a depolarizing device issued from multilayer thin film techniques. The optical properties of the coatings vary in their plane, which can be produced with classical thin film deposition techniques and non-uniformity effects [22]. A zero DOP value is then obtained through a spatial process [14, 23] resulting from

Optics EXPRESS

the transverse polarimetric phase variations of the device. The thin film design allows to control the depolarization bandwidth (broad or narrow). Advantages and limitations of the procedure are discussed including diffraction processes.

2. Principles

2.1. Spatial depolarization

Here the basic idea to depolarize light consists in the introduction of an optical device whose properties vary with its transverse coordinates r = (x,y), that is, in the plane perpendicular to its normal parallel to z (Fig. 1). More exactly, we are interested in the transverse variations of the polarimetric phase difference $\Delta\delta = \delta_s - \delta_p$ (see Fig. 1), which is known to be a key parameter for the control of light polarization [8, 9]. There are different ways to design and produce such optical device, and among them are thin film interferential filters [24] (planar multilayers); indeed transverse gradients of optical thickness can be easily produced with these techniques when one takes advantage of non-uniformity effects within the vacuum chamber [25, 26].

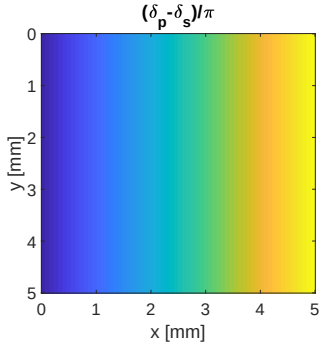

Fig. 1. Example of 1D-transverse variations of the polarimetric phase difference at the surface x-y of the device.

Consider now an incident plane wave illuminating this sample at oblique incidence i_0 from a transparent medium of refractive index n_0. The optical regime is monochromatic with the illumination wavelength λ. The device is assumed to be linear and isotropic. Since the incident light is fully polarized (one wavelength, one direction), the incident electric field E_0^+ can be described with 2 complex vectors as:

$$E_0^+ = \begin{vmatrix} E_{0s}^+ \\ E_{0p}^+ \end{vmatrix} = A_0^+ exp\,[j(\sigma_0.r + \alpha_0 Z)] \qquad with \quad A_0^+ = \begin{vmatrix} A_{0S}^+ exp(j\phi_S) \\ A_{0P}^+ exp(j\phi_P) \end{vmatrix} \tag{1}$$

where the real amplitude ratio A_{0P}^+/A_{0S}^+ and the phase difference $\Delta\Phi = \Phi_S - \Phi_P$ control the incident state of polarization. Notice here that the subscripts S and P are for transverse electric (TE or S) and transverse magnetic (TM or P) polarizations of light. The propagation (exponential) term is given versus the illumination spatial frequency ν_0, that is:

$$\sigma_0 = 2\pi\nu_0 = k sin(i_0)x \quad and \quad \alpha_0 = [k_0^2 - \sigma^2]^{0.5} = k_0 cos(i_0) \quad with \quad k_0 = 2\pi n_0/\lambda \tag{2}$$

Then at each position (x,y) on the sample the complex reflection coefficient r(x,y) is written

Optics EXPRESS

for each polarization as:

$$r_s(x,y) = \sqrt{R_s(x,y)}exp[j\delta_s(x,y)] \tag{3a}$$

$$r_p(x,y) = \sqrt{R_p(x,y)}exp[j\delta_p(x,y)] \tag{3b}$$

As a consequence, the complex reflected field E_r in the far field can be seen as the superimposition of elementary local reflections $e_r(x,y)$ of waves with complex vectors given by:

$$e_r = \begin{vmatrix} e_{rs} \\ e_{rp} \end{vmatrix} = exp[j(\sigma_0.r + \alpha_0 Z)] \begin{vmatrix} A^+_{0S}\sqrt{R_S}exp[j(\phi_S + \delta_S)] \\ A^+_{0P}\sqrt{R_P}exp[j(\phi_P + \delta_P)] \end{vmatrix} \tag{4}$$

In regard to the incident polarization, the polarization of each reflected field $e_r(x,y)$ is modified by the presence of the ratio R_p/R_s and the phase difference $\Delta\delta = \delta_S - \delta_P$, and this modification varies with the spatial location (x,y).

At this step all the elementary reflected fields are fully polarized (dop = 1), and this polarization is local and temporal. Hence since the optical regime is purely monochromatic, the only way to create depolarization is to consider a spatial depolarization process [14]. The resulting polarization degree will be denoted DOP and characterizes a spatial average, in opposition to the previous dop which is the result of a temporal average [8]. In order to reach this spatial depolarization, the polarization behavior of the field should strongly vary within the receiver aperture, and so within the illumination area of the sample. The result is a series of local and fully (temporal) polarization states whose spatial average leads to spatial depolarization in the far field.

The spatial DOP can be calculated in a way similar to the temporal one (dop), and this consists in replacing all temporal averages by spatial averages [14]. The result is the following:

$$DOP^2 = 1 - 4[\beta/(1+\beta)^2][1 - |\mu|^2] \tag{5}$$

with

$$\beta = < |E_{rp}|^2 > / < |E_{rs}|^2 > \tag{6}$$

$$\mu = < E_{rs}E^*_{rp} > / [< |E_{rs}|^2 >< |E_{rp}|^2 >]^{0.5} \tag{7}$$

where all brackets <> are for spatial averages. In these relations β and μ designate the polarization ratio and the mutual coherence. All quantities are given for the reflected field E_r. For an incident field which is parallel and fully polarized one should have:$|\mu_0| = 1 => dop_0 = 1$. The results are similar for all the elementary reflections that are fully polarized.

The final step is to combine Eqs. (2)–(4) with Eqs. (5)–(7) and quantify how the spatial variations of reflection within the illumination area reduce the polarization degree of light. However to reach this goal we first have to express in an exact way the reflected field E_r versus the series of elementary components e_r.

2.2. Reflected field

Strictly speaking one should have to use exact electromagnetic theories to relate the reflected field to the spatial variations of reflection. Indeed the reflection formulae that are classically used in thin film techniques are given for a plane wave illuminating a sample which is invariant along the (x,y) directions. In other words, diffraction theory has to be considered when light interacts with the specific device of Fig. 1. Here this point is classically solved with approximate theories issued from Huygens-Fresnel principles [27, 28] and that are currently used for propagation, diffraction and Fourier or paraxial optics. Most often these models are used for transmitted light

Optics EXPRESS

and assume that the field at the exit surface of the sample (z = 0) is equal to the incident field E_0^+ multiplied by the amplitude transmission factor t(r), that is:

$$E_t(r, z = 0) = E_0^+(r, 0)t(r) \tag{8}$$

Under this assumption the wave packet of the transmitted field at distance z can be developed for each polarization mode as follows:

$$E_t(r, z) = \int_\nu A(\nu)exp[j(2\pi\nu.r + \alpha(\nu)Z)]d\nu = F.T.[A(\nu)exp(j\alpha(\nu)Z)] \tag{9}$$

that is:

$$E_t(r, z) = F.T.[A(\nu)] *_r H(r, Z) = E_t(r, 0) *_r H(r, Z) \tag{10}$$

where $*_r$ indicates a convolution product versus r, F.T. is a Fourier transform and H(r,z) is a Huygens Fresnel propagator [27, 28]:

$$H(r, Z) = F.T.\{exp[j\alpha(\nu)Z]\} \tag{11}$$

At this step the field at the surface sample results from the Huygens assumption, that is:

$$E_t(r, 0) = t(r)E_0^+(r, 0) = t(r)exp(j\sigma_0.r)A_0^+ \tag{12}$$

Equations (10) and (12) yield:

$$E_t(r, Z) = A_0^+ t(r)exp(j\sigma_0.r) *_r H(r, Z) \tag{13}$$

which can also be written in the Fourier plane as:

$$\hat{E}_t(\nu, Z) = A_0^+ \hat{t}(\nu - \nu_0)exp[j\alpha(\nu)Z] \tag{14}$$

The case of reflection is similar and leads to:

$$E_r(r, Z) = A_0^+ r(r)exp(j\sigma_0.r) *_r H(r, -Z) \tag{15}$$

$$\hat{E}_r(\nu, Z) = A_0^+ \hat{r}(\nu - \nu_0)exp[-j\alpha(\nu)Z] \tag{16}$$

with δ the Dirac function.

These last Eqs. (15) and (16) allow to calculate the reflected field E_r from the knowledge of the spatial variations of reflection at the sample entrance.

2.3. Polarization ratio and mutual coherence

The Poynting flux vector from a wave packet can be directly expressed from the field expression [27], provided that the receiver aperture collects the whole flux. Following Eq. (16) the result for the reflected flux is:

$$\Phi = |A_0^+|^2(1/2\omega\mu) \int_\nu \alpha(\nu)|\hat{r}(\nu - \nu_0)|^2 d\nu \tag{17}$$

In case of slight beam divergence, Eq. (17) is reduced to:

$$\Phi = |A_0^+|^2(\alpha_0/2\omega\mu) \int_\nu |\hat{r}(\nu - \nu_0)|^2 d\nu \tag{18}$$

so that the Fourier reflection spectrum becomes the key quantity. Now using Parseval theorem the flux can also be written versus the spatial variations of reflection:

Optics EXPRESS

$$\Phi = |A_0^+|^2(\alpha_0/2\omega\mu)\int_r |r(r)|^2 dr \tag{19}$$

Hence the polarization ratio and the mutual coherence which give the spatial polarization degree as a spatial average (see Eqs. (5)–(7)) can be written as:

$$\beta = \beta_0 \left(\int_r |r_p(r)|^2 dr\right) / \left(\int_r |r_s(r)^2| dr\right) \tag{20}$$

$$\mu = \int_r r_s(r) r_p^* dr / \left\{\left(\int_r |r_s(r)|^2 dr\right)\left(\int_r |r_p(r)|^2 dr\right)\right\}^{0.5} \tag{21}$$

with

$$\beta_0 = < |A_{0p}^+|^2 > / < |A_{0s}^+|^2 > \tag{22}$$

Equations (20) and (21) coupled to Eqs. (5)–(7) now allow to calculate the spatial polarization degree versus the spatial variations of reflection, and the results takes into account the diffraction process. Notice that these formulae are given for an incident plane wave (full incident temporal polarization).

2.4. Stokes parameters

We still work with full polarization of the incident light. The spatial DOP of reflection will be calculated in the next sections from Eqs. (5)–(7) and Eqs. (20)–(22). However it will also be necessary to associate a polarization state to each polarization degree, that is, a location on the Poincaré sphere. For that we use classical Stokes parameters [8] whose values S_i are defined as:

$$\begin{array}{ll} S_0 = < |E_s|^2 + |E_p|^2 > & S_1 = < |E_s|^2 - |E_p|^2 > \\ S_2 = < E_s E_p^* + E_s^* E_p > & S_3 = j < E_s E_p^* - E_s^* E_p > \end{array} \tag{23}$$

where (*) is for complex conjugation and $j^2 = -1$. The parameters are then normalized by S_0 so as to introduce a sphere of unity radius. All data of the sphere are given versus spherical coordinates extracted from the S_i values [8]. Notice that the polarization degree can also be calculated from these values as:

$$dop^2 = (1/S_0)^2(S_1^2 + S_2^2 + S_3^2) \tag{24}$$

In the case of plane waves (dop = 1), the Stokes parameters s_i are immediate to write, that is:

$$\begin{array}{ll} s_0 = 1 & s_1 = (1-\beta)/(1+\beta) \\ s_2 = 2cos(\psi)\sqrt{(\beta)}/(1+\beta) & s_3 = -2sin(\psi)\sqrt{(\beta)}/(1+\beta) \end{array} \tag{25}$$

with, in the case of incident light:

$$\psi = \phi_s - \phi_p \qquad and \qquad \beta = \beta_0 = |A_{0p}^+/A_{0s}^+|^2 \tag{26}$$

and for the elementary reflections:

$$\psi = (\phi_s - \phi_p) + (\delta_s - \delta_p) \qquad and \qquad \beta = \beta_0 R_p/R_s \tag{27}$$

Equations (26) and (27) describe full polarization states associated with locations at the surface of the Poincaré sphere.The linear states of polarization are on the equator, the circular states of polarization are at the poles of the sphere and the elliptical states are arbitrary located at the surface of the sphere for polarized light. On the other hand, partial polarization is described

Optics EXPRESS

with Stokes parameters associated with location within the volume of the sphere. Now for the integrated spatial DOP the Stokes parameters are given by:

$$\begin{array}{ll} s_0 = 1 & s_1 = (1-\beta)/(1+\beta) \\ s_2 = 2Real(\mu)\sqrt{(\beta)}/(1+\beta) & s_3 = -2Im(\mu)\sqrt{(\beta)}/(1+\beta) \end{array} \tag{28}$$

where β and μ must be taken from Eqs. (20)–(22).

3. Numerical calculation with deterministic polarimetric phases

The spatial DOP depends on the spatial variations of reflection, both in phase and modulus. For the sake of simplicity we start with the situation where the modulus of reflection are identical for both polarizations on the whole sample, that is:

$$R_s = |r_s|^2 = R_p = |r_p|^2 \tag{29}$$

One practical way to hold this condition would be to work under total internal reflection ($R_s = R_p = 1$), but this can also be obtained in a broad-band spectral region with the superimposition of multi-dielectric mirrors.

3.1. Case where $\beta_0 = 1$

We first consider the situation where the incident wave follows $\beta_0 = 1$, which corresponds to having as much energy on the s-axis as on the p-axis. Then according to Eqs. (20) and (29) we also have $\beta = 1$ for the reflected field, so that the key parameter which controls the spatial polarization becomes the mutual coherence:

$$\beta = 1 \Rightarrow DOP = |\mu| \tag{30}$$

with

$$\mu = \int_r r_s(r) r_p^*(r) dr \Big/ \left\{ \left(\int_r |r_s(r)|^2 dr \right) \left(\int_r |r_p(r)|^2 dr \right) \right\}^{0.5} \tag{31}$$

At this step one can emphasize the role of the polarimetric phase $\Delta\delta = \delta_s - \delta_p$. Indeed under the approximation that R_s and R_p are constant over the sample surface, Eq. (31) can be rewritten as:

$$\mu = (1/\Sigma) \int_{x,y} exp[j\Delta\delta(x,y)] dxdy = < exp[j\Delta\delta(x,y)] >_{x,y} \tag{32}$$

with Σ the illumination area. Hence we conclude that the correlation between the polarimetric reflection phases plays a major role. In the case of deterministic phase functions, specific extreme values of the phase can be enough to cancel the DOP. Indeed let us still consider a fully polarized incident beam with $\beta_0 = 1$, and assume that the filter reflection exhibits spatial variations which are linear versus one coordinate (see Fig. 1), that is:

$$\Delta\delta(x,y) = \Delta\delta_0 + \gamma x \tag{33}$$

with $\Delta\delta_0$ a phase origins and γ the phase slope. Following Eq. (33), Eq. (32) becomes:

$$\mu = exp(j\Delta\delta_0) sin(\gamma L/2)/(\gamma L/2) = exp(j\Delta\delta_0) sinc(\gamma L/2) \tag{34}$$

with L the length of the squared illumination ($\Sigma = L^2$). Hence the final DOP of the reflected field is a sinc function:

Optics EXPRESS

$$DOP = |sinc(\gamma L/2)| \tag{35}$$

Equation (35) shows that the DOP can be controlled with the slope of the polarimetric phase, with zero values given by $L_k = k2\pi/\gamma$. However such slope is not easy to control, for which reason one should work with high slope values or large illumination areas in order to reduce the DOP. Typically a value $\gamma L > 4\pi$ ensures a DOP lower than 5%. Notice that these results can be directly extended to the case of linear variations versus both coordinates x and y. Equation (35) would then be rewritten as:

$$DOP = |sinc(\gamma_x L_x/2)sinc(\gamma_y L_y/2)| \tag{36}$$

with γ_x and γ_y the slopes along x and y, and $\Sigma = L_x L_y$ the area of the rectangular illumination region.

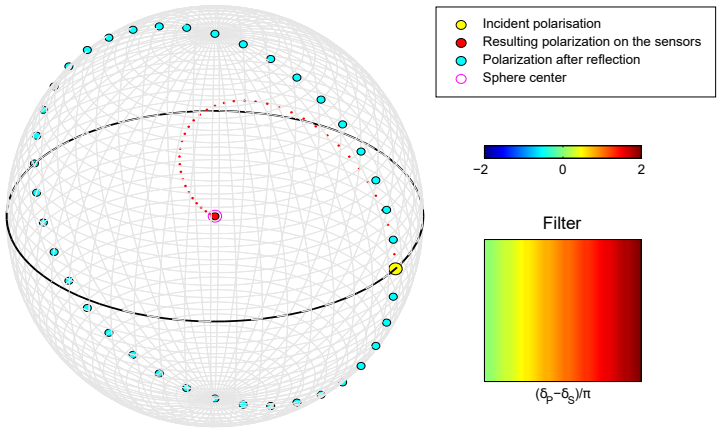

Fig. 2. Incident, local and global polarizations plotted on the Poincaré sphere with $\gamma = \pi/20$.

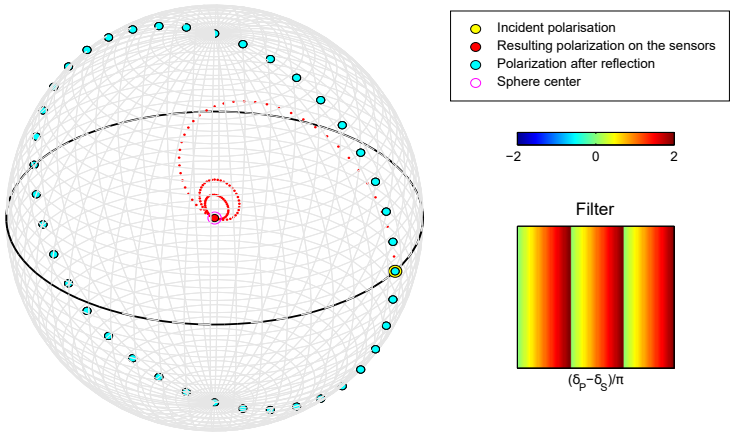

Fig. 3. Incident, local and global polarizations plotted on the Poincaré sphere with $\gamma = \pi/60$.

Results are shown in Fig. 2 for a linear slope along x. The incident polarization state if located by a yellow dot on the sphere. The full polarization states of the elementary (local) reflections are also given in blue dots and describe a circle at the sphere surface, whose center is the center of

Optics EXPRESS

the sphere. Then the red curve gives the integrated spatial DOP versus the integration area. The greater this area, the lower is the DOP. The DOP is unity for a local reflection, and then decreases to zero with large L values. The behavior of this decrease is similar to loops because of the Sinc function. The final DOP is for the integration over the whole sample; its zero value at the sphere center characterizes a total depolarization. Figure 3 is analogous to Fig. 2 but the slope is greater, for which reason several loops can be seen. More accuracy is given to the DOP with greater values of slope and area.

3.2. Case where $\beta_0 \neq 1$

Now we have to consider the case of a general incident elliptical polarization with $\beta \neq 1$. Following again Eqs. (5), (20) and (22), the DOP modification can be emphasized as below:

$$DOP = 1 - 4\left\{\beta_0/(1+\beta_0)^2\right\}\left[1 - DOP_1^2\right] \tag{37}$$

where DOP_1 is the polarization degree of the previous sub-section calculated with $\beta_0 = 1$. It is easy to check that this new DOP cannot be set to zero unless with $\beta_0 = 1$. Therefore in this case only a DOP reduction can be achieved and the spatial depolarization will be more efficient around unity β_0 values. The minimum DOP is given as:

$$DOP_{min} = [(1-\beta_0)/(1+\beta_0)]^2 \tag{38}$$

Results are given in Fig. 4 in case where $\beta_0 = 0.5$. In a way similar to Fig. 2, the incident polarization is located by the yellow dot at the surface of the sphere. The local sample reflections have polarizations located by the blue dots at the surface of the sphere. We observe that these blue dots again describe a circle, but the center of this circle is different from that of the sphere. The minimum DOP is obtained at the center of the circle, which is the barycenter of the blue dots.

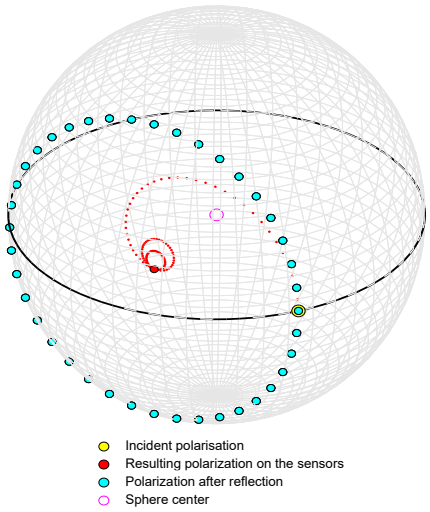

Fig. 4. Incident, local and global polarizations plotted on the Poincaré sphere with $\gamma = \pi/60$ for an arbitrary elliptical incident polarization (see text) with $\beta \neq 1$.

3.3. Case of random phase variations

Another way to reduce the DOP is to replace the linear variations by random variations, that is:

$$\Delta\delta(x,y) = \Delta\delta_0 + RD(x,y) \tag{39}$$

Optics EXPRESS

with RD a random signal versus the x location on the sample. Such phase distribution could be reached for instance with a photosensitive device under speckle illumination. In Fig. 5 below we considered RD(x) as a white noise uniformly distributed between $[0; 2\pi]$. The incident polarization is again given with $\beta = 1$, and is associated with a yellow dot in the Fig. 5 at the surface sphere. The blue dots are given at the sphere surface and represent the random polarization states at the surface sphere. These blue dots cover the sphere in a uniform way. Then their averages give the red dots which characterize the spatial DOP. In comparison to the previous deterministic phase variations, Fig. 5 shows that the convergence process is different with a random distribution.

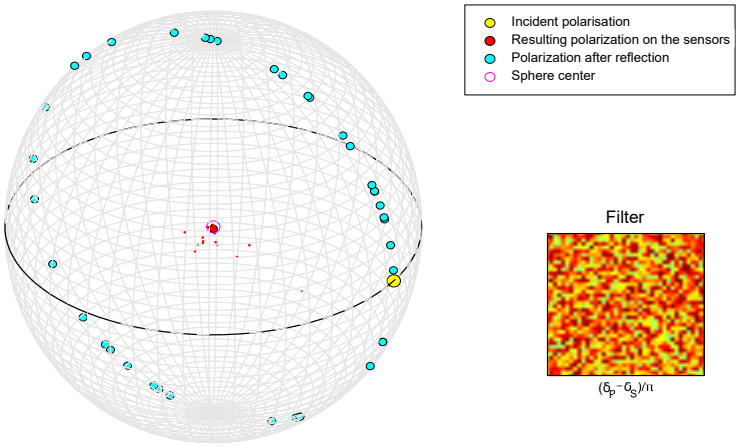

Fig. 5. Incident, local and global polarizations plotted on the Poincaré sphere with a random phase distribution (For greater clarity, only the polarizations corresponding to the first line of the filter are plot).

4. Introduction of thin film multilayers

Optical coatings are now introduced as the devices which create the polarimetric phase variations. These coatings are known to be highly polarizing at oblique incidence [29–32], and we will take advantage of non-uniformity effects [22, 29] to reach a gradient of these properties at the surface sample. This will allow to start a practical study of the depolarizer performances, including its wavelength variations. In other words, the coating design and its thickness gradient will drive the wavelength variations of the polarization degree.

4.1. Thickness non-uniformity

The spatial variations of reflection are here assumed to originate from a non-uniformity effect which can be created during production of the films [22, 25, 33, 34]. The simplest geometry is that of a sample positioned within the vacuum chamber in such a way that thickness non-uniformity is enhanced at its surface (Fig. 6), which has to be related to the emission diagram of the sputtered or evaporated materials. Strictly speaking one should also take account of a modification of refractive index resulting from an oblique growth of materials, as well as from substrate rotation. Also, uniformity should be the same for all materials. However such technique has been largely validated to produce high quality linear filters, that is, narrow-band filters whose central wavelength λ_0 linearly varies with position (x,y) at their top surface [22, 25, 33, 34]. Other techniques exist and involve different moving masks elaborated to control the uniformity. Depending on the coating sensitivity and the required application, the uniformity variations can be negligible or not. Previous results have also shown how these variations could be corrected in

Optics EXPRESS

narrow-band filters via photosensitive effects [35]. We define the uniformity function $u(x, y)$ as the ratio of material thickness $e(x, y)$ deposited at one position (x, y) of the sample, in regard to the thickness deposited at one reference position $(0, 0)$, that is:

$$u(x, y) = e(x, y)/e(0, 0) = e(x, y)/e_0 \tag{40}$$

Such function is related to the deposition technology and to the geometry of the vacuum chamber. In what follows we consider the simplest but realistic situation where the thickness variations are linear versus one transverse x-direction at the sample surface (see Fig. 7). This 1-D thickness gradient is written for each layer as:

$$e_i(x, y) = e_i(x) \approx e_{i,0} + xtan(\kappa) \tag{41}$$

with κ the angle shown in Fig. 7, and $0 < x < L$, with L the dimension of the illuminated area. This gives the uniformity as:

$$u_i(x, y) = 1 + (x/e_{i,0})tan(\kappa) \tag{42}$$

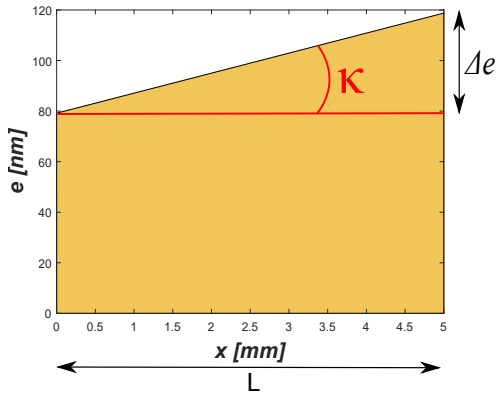

Fig. 6. Draft on non-uniformity effects at the surface sample (see text).

4.2. Non-uniformity in quarter-wave stacks

Now one basic idea to produce linear filters relies on the fact that most coatings are made with quarter-wave layers [29–32]. These layers follow:

$$(necos\theta)_i = q_i\lambda_0/4 \tag{43}$$

with $(ne)_i$ the optical thickness of layer (i), and θ_i the refraction angle within layer (i). Most often two dielectric materials are used, that are a high index (H) and a low-index (L) material. Hence multi-dielectric quarter-wave mirrors $(M2p + 1)$ follow a simple design given by:

$$M_{2p+1} = Air/(HL)^p H/Substrate \tag{44}$$

with $2p + 1$ the number of layers, and H and L represent quarter-wave layers matched for oblique incidence:

$$(necos\theta)_H = (necos\theta)_L = \lambda_0/4 \tag{45}$$

As shown in Fig. 7, such designs provide dielectric mirrors with a central wavelength λ_0 and a band-pass [36] given by:

Optics EXPRESS

$$\Delta f/f_0 = (4/\pi)arcsin[(\tilde{n}_H - \tilde{n}_L)/(\tilde{n}_H + \tilde{n}_L)] \quad (46)$$

with $f = 2\pi c/\lambda$ the temporal frequency, $\tilde{n}$ the effective index defined by $\tilde{n} = n\alpha/k$ in TE polarization mode and $\tilde{n} = nk/\alpha$ in TM polarization mode, with $\alpha^2 = k^2 - \sigma^2$.

Now taking into account the uniformity function $u(x)$, the optical thicknesses given in (44) are modified at the surface sample as:

$$n_H e_H(x)cos\theta_H = u_H(x)\lambda/4 \quad and \quad n_L e_L(x)cos\theta_L = u_L(x)\lambda/4 \quad (47)$$

with

$$u_H(x) = 1 + (x/e_H)tan(\kappa) \quad and \quad u_L(x) = 1 + (x/e_L)tan(\kappa) \quad (48)$$

At this step we consider a first-order approximation, thanks to the low thickness variations that will be considered, that is:

$$u_H(x) \approx u_L(x) \approx u_(x) \quad (49)$$

Under these conditions, any lack of uniformity at the surface coating will shift its central wavelength λ_0 to another one $\lambda_0(x)$ given by:

$$\lambda_0(x) = u(x)\lambda_0 = \lambda_0[1 + (x/e)tan(\kappa)] \quad (50)$$

with $e = (e_H + e_L)/2$ These effects are recalled in Figs. 7(a) and 7(b) with a central coating $M_{15} = Air/(HL)^7 H/Substrate$ designed for a 45° illumination at $\lambda_0 = 633nm$, with Ta_2O_5/SiO_2 materials. The shifted coatings show similar properties but the central wavelengths result from uniformity values $u(x1 = 0mm) = 1$, $u(x2 = 10mm) = 1.1$ and $u(x3 = 20mm) = 1.2$. It should here be noticed that the optical properties are just shifted (but not modified), but this is valid under the assumption of a slight difference between the uniformity of the two materials ($u_H \approx u_L$), which is an accurate first-order approximation. The technique can be directly extended to narrow-band filters whose cavity layer is a half-wave layer.

4.3. Impact of uniformity on depolarization

Now we come back to depolarization. As in Section 3.1, we limit ourselves to the case $\beta_0 = 1$. The spatial dop is again calculated according to Eqs. (5)–(7) for a 1D geometry, that is:

$$DOP^2 = 1 - 4[\beta/(1+\beta)^2][1 - |\mu|^2] \quad (51)$$

where the mutual coherence μ and the polarization ratio β of the reflected field follow:

$$\mu = \int_x r_s(x)r_p^*(x)dx \Big/ \left(\left[\int_x |r_s(x)|^2 dx\right]\left[\int_x |r_p(x)|^2 dx\right]\right)^{0.5} \quad (52)$$

$$\beta = \beta_0 \left[\int_x |r_p(x)|^2 dx\right] \Big/ \left[\int_x |r_s(x)|^2 dx\right] \quad (53)$$

Actually the reflection coefficient $r(x)$ at position x on the sample is nothing else than the reflection coefficient $r[\lambda, \lambda_0(x)]$ calculated at wavelength λ for the quarter-wave stack designed at the central wavelength $\lambda_0(x)$, with:

$$\lambda_0(x) = u(x)\lambda_0 = \lambda_0[1 + (x/e)tan(\kappa)] \quad (54)$$

Therefore Eqs. (52) and (53) can be rewritten as:

Optics EXPRESS

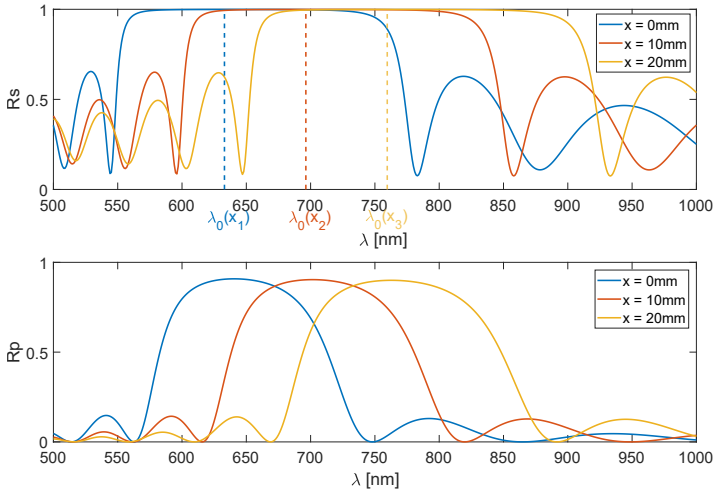

(a) Optical properties of a quarter-wave mirror at the central wavelength $\lambda_0(x)$ and 45° incidence, with non-uniformities equal to $u_1 = 1$, $u_2 = 1.1$ and $u_3 = 1.2$ (see text). The top and bottom Figs. are for TE and TM polarizations respectively. We observe a single shift of the optical properties.

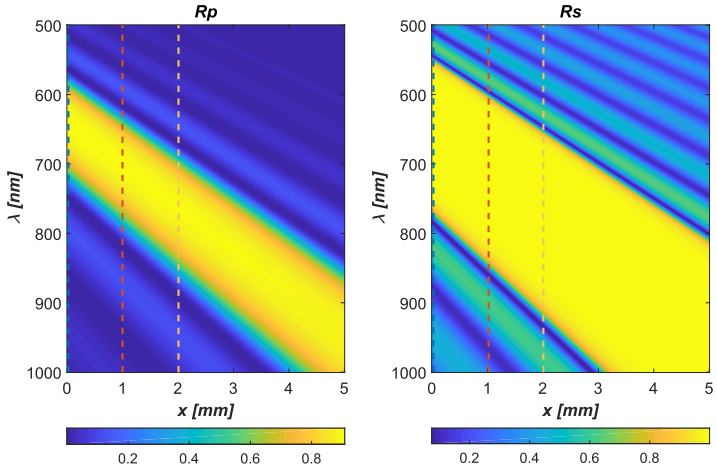

(b) General view of the impact of non-uniformity on a quarter-wave multi-dielectric mirror (see text). The left and right Figs. are for TM and TE polarizations respectively. The band-pass is polarization dependent, and is shifted with the x-position.

Fig. 7. Optical properties of a quarter-wave mirror at the central wavelength $\lambda_0(x)$ and 45° incidence

Optics EXPRESS

$$\mu(\lambda) = \int_x r_s(\lambda, \lambda_0(x)) r_p^*(\lambda, \lambda_0(x)) dx \Big/ \left(\left[\int_x |r_s(\lambda, \lambda_0(x))|^2 dx \right] \left[\int_x |r_p(\lambda, \lambda_0(x))|^2 dx \right] \right)^{0.5} \quad (55)$$

$$\beta = \beta_0 \left[\int_x |r_p(\lambda, \lambda_0(x))|^2 dx \right] \Big/ \left[\int_x |r_s(\lambda, \lambda_0(x))|^2 dx \right] \quad (56)$$

These results emphasize the fact that the spatial DOP behavior results from the specific spectral properties of the reflection function $r[\lambda, \lambda_0(x)]$. However another thin film property can also be introduced to go further in the analytical formalism. For dielectric films the index dispersion is slight in the visible range so that one can consider that all previous quarter-wave mirrors $M15(x)$ have identical optical properties after centering at the same design wavelength λ_0. This allows to write, for each polarization:

$$r[\lambda, \lambda_0(x)] = r_0[\lambda - (\lambda_0(x) - \lambda_0), \lambda_0] = r_0[\lambda - (u(x) - 1), \lambda_0] \quad (57)$$

with r_0 the reflection function of the mirror at $x = 0$, designed at the central wavelength λ_0. In other words, we do not have any more to consider the reflection function r of a coating whose design is x-dependent, since all calculation can be drawn with the r_0 function designed for $\lambda_0(x = 0) = \lambda_0$. Owing to this result, Eqs. (52) and (53) can be rewritten with a unique reflection function r_0 as:

$$\mu(\lambda) = \int_x r_{0s}[\lambda - \lambda_0'(x)] r_{0p}^*[\lambda - \lambda_0'(x)] dx \Big/ \left(\left[\int_x |r_{0s}[\lambda - \lambda_0'(x)]|^2 dx \right] \left[\int_x |r_{0p}[\lambda - \lambda_0'(x)]|^2 dx \right] \right)^{0.5} \quad (58)$$

$$\beta(\lambda) = \beta_0 \left[\int_x |r_{0p}[\lambda - \lambda_0'(x)]|^2 dx \right] \Big/ \left[\int_x |r_{0s}[\lambda - \lambda_0'(x)]|^2 dx \right] \quad (59)$$

with

$$\lambda_0'(x) = \lambda_0(x/e) tan(\kappa) \quad (60)$$

4.4. Loss-less depolarization band-pass

These last Eqs. (58)–(60) give the spectral variations of the polarization degree versus the λ_0 coating design and versus the uniformity. At this step it is major to analyze in which bandwidth BW depolarization may occur without losses. For that the global polarization ratio should be high ($\beta(\lambda) \approx 1$) in this bandwidth BW, while the mutual coherence should approach zero in the same bandwidth BW, due to a rapid variation of the polarimetric phase. In order to keep a high polarization ratio, the argument of the reflection functions in Eq. (59) would remain within the intrinsic mirror bandwidth $\Delta\lambda$ given by Eq. (46), that is:

$$\lambda_0 u(x) - \Delta\lambda/2 < \lambda < \lambda_0 u(x) + \Delta\lambda/2 \qquad for \;\; 0 < x < L \quad (61)$$

Actually $\Delta\lambda$ here represents the intersection of the two polarizations bandwidths, so that oblique incidence can be considered. This gives the general condition:

$$\lambda_0 u(L) - \Delta\lambda/2 < \lambda < \lambda_0 u(0) + \Delta\lambda/2 \quad (62)$$

That is:

$$\lambda_0 u(L) - \Delta\lambda/2 < \lambda < \lambda_0 + \Delta\lambda/2 \quad (63)$$

Optics EXPRESS

with

$$u(L) = 1 + (L/e)tan(\kappa) \tag{64}$$

Therefore the width of the depolarization band-pass is given by:

$$BW = \Delta\lambda - \lambda_0(L/e)tan(\kappa) = \Delta\lambda - \lambda_0\Delta e/e \tag{65}$$

where Δe is the maximum thickness variation taken at $x = L$ (see Fig. 6). This bandwidth is centered at the wavelength:

$$\lambda_{00} = (\lambda_0/2)[1 + (L/e)tan(\kappa)] = (\lambda_0/2)[1 + \Delta e/e] \tag{66}$$

Since the band-pass must be positive, Eq. (65) implies that:

$$(L/e)tan(\kappa) = \Delta e/e < \Delta\lambda/\lambda_0 \tag{67}$$

Such condition depends on the uniformity parameters and must be full-filled to allow a loss-less depolarization bandwidth to occur with a x-gradient quarter-wave mirror. Typically for our quarter-wave stacks the ratio $\Delta\lambda/\lambda_0$ of band-pass to wavelength is of the order of 0.22 for R_S and 0.15 for R_P, so that a value $\Delta e/e < 0.1$ would be enough to guarantee the condition $\beta \approx 1$. This is shown in Fig. 8 where the red curve is calculated for $\Delta e/e = 1\%$ and emphasizes a high β value band-pass in the spectral range $600nm - 700nm$. On the other hand the orange curve is given when Eq. (67) is not satisfied ($\Delta e/e = 1\%$) and shows no β band-pass. However we cannot forget that $\beta \approx 1$ is only a necessary condition for total depolarization, and that the device should also exhibit a zero mutual coherence ($\mu \approx 0$). Actually to satisfy Eq. (67) the thickness slope κ must be low ($\Delta e < e/10$), but this low value minimizes the x-gradient and reduces the mirror to a quasi-flat mirror (no significant phase variations versus x-position). This is the reason why such device does not depolarize light, as shown by the blue dashed line plotted in Fig. 8. So we here conclude that this gradient mirror is not adequate to depolarize light in a broad-band region. Furthermore, another major difficulty with this technique arises from the fact that both bandwidth BW and central wavelength λ_{00} vary with the spot size (L) and uniformity slope (κ), which leads us to propose an alternative device in the next section.

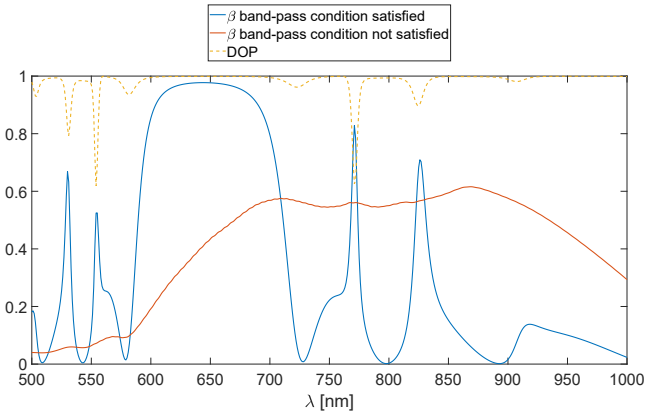

Fig. 8. Spectral variations of polarization ratio (full lines) in situations where the band-pass condition Eq. (67) is satisfied (blue curve) or not (orange curve). The polarization degree (yellow dashed curve) is also plotted in the case where the bandpass condition is satisfied (see text).

Optics EXPRESS

5. Introduction of a second additional (flat) mirror

One solution to face these difficulties consists in the introduction of an additional quarter-wave mirror M_{add} with no x gradient. The resulting mirror (see Fig. 9) will be the superimposition of this flat mirror M_{add} and the previous gradient mirror $M_0(x)$, that is:

$$M(x) = Air/M_0(x)M_{add}/substrate \tag{68}$$

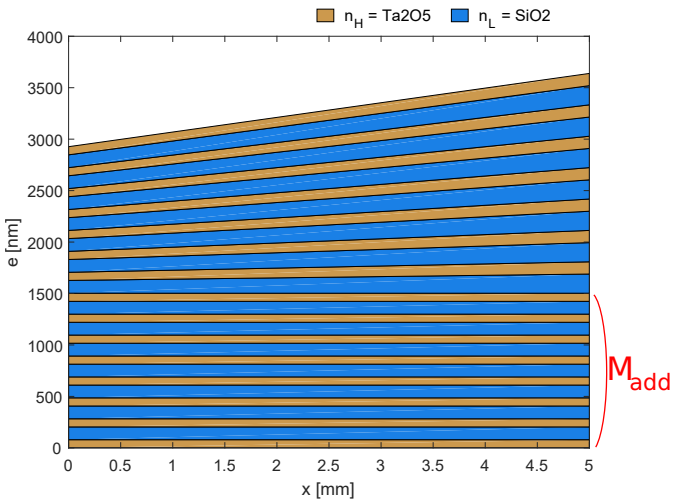

Fig. 9. Case where the gradient mirror $M_0(x)$ is deposited on a flat mirror M_add (see text).

5.1. Constant intensity bandwidth

Here we consider that M_{add} and $M_0(0)$ have identical central wavelength λ_0. Because M_{add} is not x-dependent, it will guarantee a high intensity reflection of the resulting mirror $M(x)$ for both polarizations ($\beta \approx 1$) in the classical bandwidth $\Delta\lambda_{add}$ of M_{add}. This is shown in Fig. 10, where the superimposition of M_{add} and $M_0(x)$ does not modify the intensity reflection factor of M_{add} in its bandwidth $\Delta\lambda_{add}$, but only the phases. Actually in this Fig. the horizontal bandwidth is for M_{add}, while the oblique one is for $M_0(x)$. Therefore there is one intensity bandwidth (M_{add}) which is now constant versus x-position, so that the reflection modulus of $M(x)$ is no more x-dependent in this bandwidth, where we can write:

$$r_{pol}(\lambda, \lambda_0(x)) \approx |r_{pol}(\lambda, \lambda_0)| exp[j\delta_{pol}(x)] \tag{69}$$

with r_{pol} the reflection function of $M(x)$. This property makes $\beta \approx 1$ over the whole illumination area in a constant bandwidth $\Delta\lambda_{add}$, so that a loss-less depolarization device can be addressed in this bandwidth. We notice here that this intensity bandwidth does not depend on the uniformity (given by L and κ parameters), which solves the problem we had to face in the absence of M_{add} in the previous section.

5.2. Mutual coherence

In a last step we analyze again the mutual coherence μ which is required for total depolarization. Indeed since $\beta \approx 1$, the spatial DOP is given by $|\mu|$ in the bandwidth $\Delta\lambda_{add}$, and this μ parameter can be set to zero if the phase variations are rapid. It is well known that the phase of quarter-wave stacks is quasi-linear versus wavelength in the reflection bandwidth. This linear behavior would

Optics EXPRESS

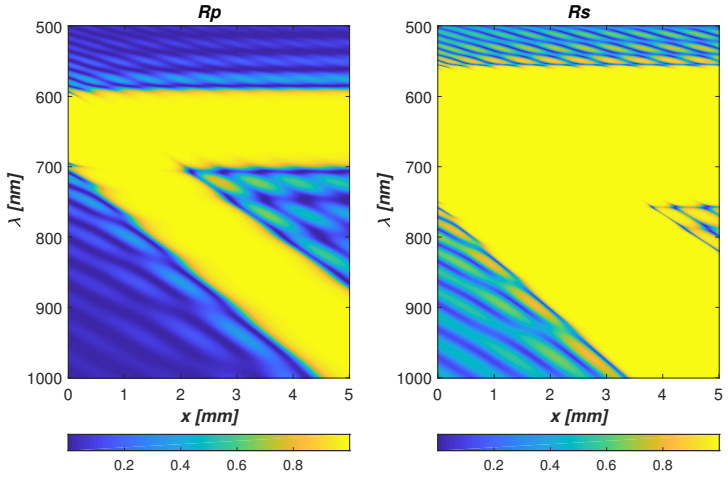

Fig. 10. Intensity spectrum of the total mirror $M(x)$, versus wavelength and x position. We observe that an intensity (horizontal) bandwidth is hold whatever the x-position. The left and right figures are given for TM and TE polarizations, respectively. The oblique bandwidth is that of the gradient mirror $M_0(x)$.

be expected not to be different versus the x position; if this were true, and following Eqs. (32) and (35), the DOP would be controlled by the phase slope γ as:

$$DOP = (1/L)\left|\int_x exp[j\Delta\delta(x)]dx\right| = |sinc(\gamma L/2)| \tag{70}$$

with $\Delta\delta = \Delta\delta_0 + \gamma x$. However as shown in Fig. 11(a) plotted for wavelength $\lambda = 695nm$, the linear behavior is first hold for $x < 1.6mm$ but shows more complex variations for $x > 1.6mm$. Therefore Eq. (70) cannot be used, but this non-linear behavior does not either prevent the mutual coherence to be cancelled; indeed the rapid and large phase variations within the whole illuminated area are enough to cancel the mutual coherence. A complete mapping of the phase is given versus wavelength (λ) and position (x) in Fig. 11(b).

5.3. Depolarization

These results allow to reach the high depolarization observed in Fig. 12. In this Fig. 12 the spatial DOP is plotted versus wavelength for different uniformities characterized by $\Delta e/e$ ranging from 0% to 100%. The reflection spectrum of the gradient mirror $M_0(x)$ is also plotted versus wavelength in dashed line. P-polarization was chosen for this spectrum since it forces the narrower bandwidth. One can see that in the $M_0(x)$ mirror band-pass, the DOP remains unity (red curve in full line) for low uniformity in the whole spectral range. Then it decreases when uniformity increases, and the final result is a total depolarization obtained in the whole bandpass when $\Delta e/e > 75\%$. We notice that the final DOP is in phase opposition with the mirror reflection. Hence the conclusion is that such devices allow to reach total depolarization of light without losses in a broad-band spectral region. The reason is that the flat mirror M_{add} forces the intensity bandwidth while the gradient mirror forces the phase bandwidth, so that both mirrors used together provide the adequate device.

Optics EXPRESS

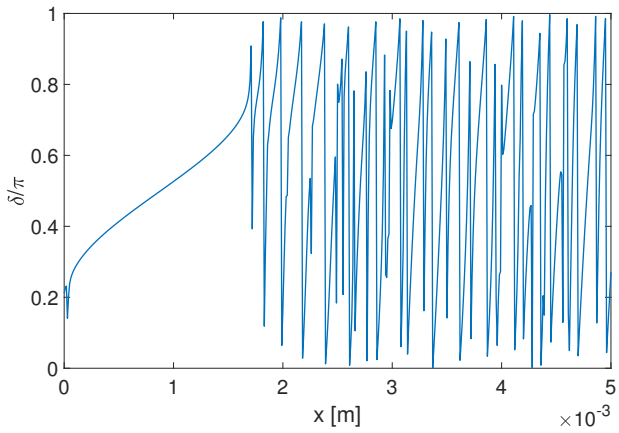

(a) Polarimetric phase variations of the total mirror $M(x)$ versus the x position, for a wavelength in the β band-pass ($\beta \approx 1$). The illumination wavelength is $\lambda = 695nm$.

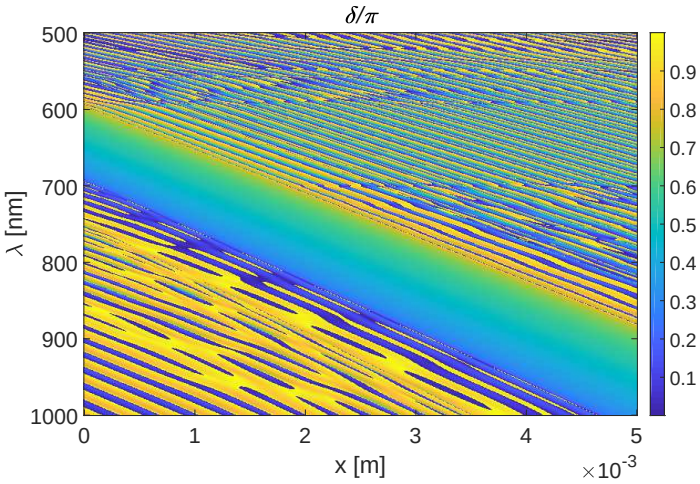

(b) Polarimetric phase difference versus x-position and wavelength for the mirror of Fig. 11(a).

Fig. 11. Polarimetric phase variations of the total mirror $M(x)$

5.4. The case of Fabry-Perot filters

This technique can be generalized to other situations where depolarization must occur in a narrow bandwidth, a specification different from the previous mirror one. To reach this result we use a specific narrow-band filter (FP) with central wavelength λ_0. The design is a flat mirror (M21) overcoated with a gradient multilayer consisting in a $2L$ spacer layer and another mirror M6, that is: $FP = Air/M6(x)/2L(x)/M21/Substrate$. The illumination incidence is 60° and materials are Ta_2O_5/SiO_2. In Fig. 13 we observe that the DOP is zero at the central wavelength while the polarization ratio is high, which characterizes a loss-less depolarization. These results are successful and confirm the generalization of the procedure to depolarize light at will in arbitrary bandwidths.

Optics EXPRESS

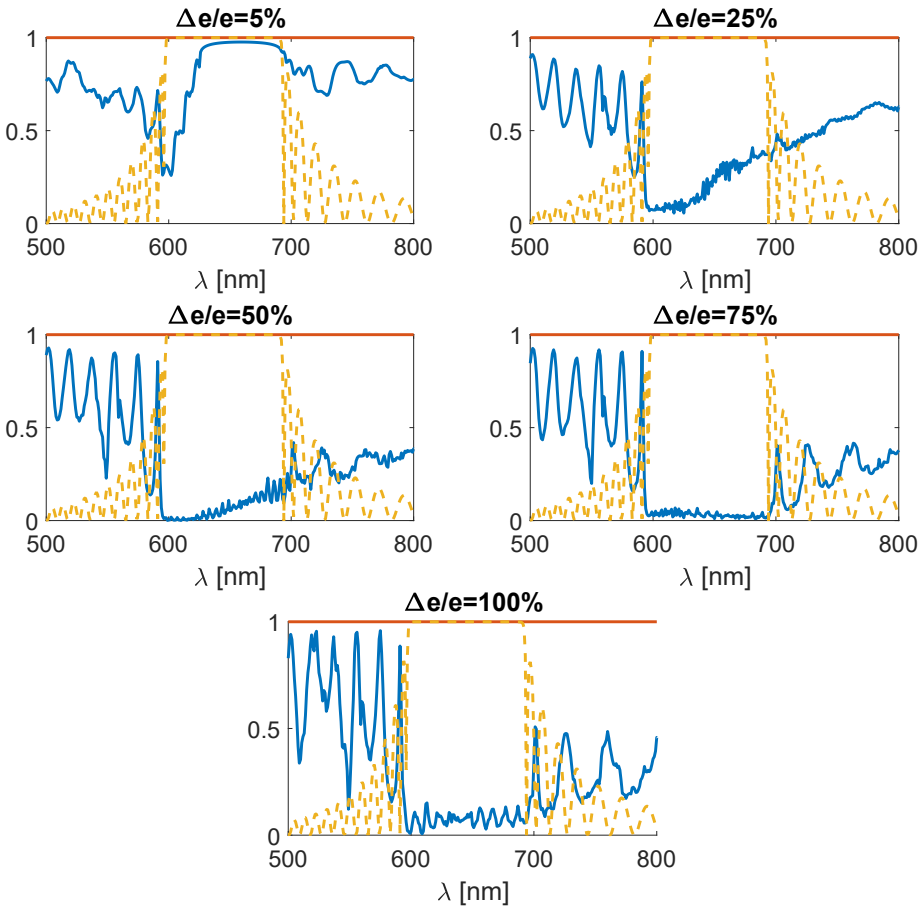

Fig. 12. Spectral variations of the polarization degree of the total mirror M(x), for different uniformity values which correspond to: $\Delta e/e$ = 5%, 25%, 50%, 75% and 100%. Total depolarization is reached in the whole mirror band-pass. The reflection spectrum of the gradient mirror is also is plotted in dashed line (see text).

6. Diffraction effects

Now we discuss diffraction processes which accompany the depolarizing device, and that should be prevented or controlled. Indeed applications require to depolarize light without losses but also without altering its wave-front. For that one can use Eqs. (15) or (16), depending on whether there is an imaging system between the sample and the detector. For the sake of simplicity we will here focus on Eq. (16) which describes a proportionality between the Fourier transforms of the field (versus x) and the reflection coefficient at a given z position and a given wavelength λ, that is:

$$\widehat{E}_r(\lambda, \nu, z) = A_0^+ \widehat{r}(\lambda, \nu - \nu_0) e^{-j\alpha(\lambda,\nu)z} \tag{71}$$

As was done in Section 5, we take into account the spatial variations of reflection within the sample plane. We consider the case of the double mirror $M(x) = M_0 + M_{add}$ which provides a controllable loss-less depolarization bandwidth. The amplitude reflection is written again for each polarization as $r_{pol}(\lambda, x)$, and we calculate its Fourier transform versus x as:

$$\widehat{r}(\lambda, \nu) = \int_x r_{pol}(\lambda, x) exp(-2\pi\nu x) dx \tag{72}$$

Optics EXPRESS

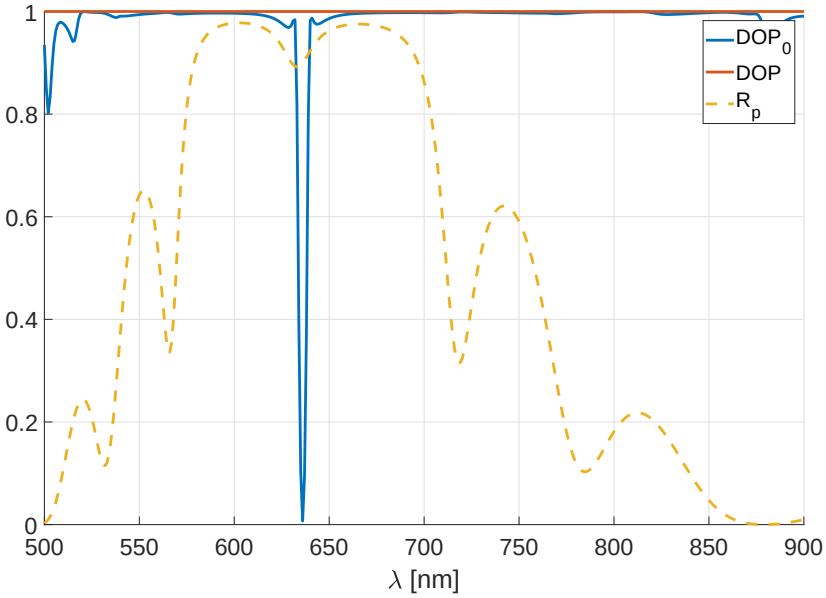

Fig. 13. Spectral variations of the polarization degree of a narrow-band filter (see text). The green curve is for the flat coating while the red curve is for the gradient coating.

Since we are interested in a modification of an intensity pattern, we consider the square quantity:

$$R(\lambda, \nu) = |\widehat{r}(\lambda, \nu)|^2 \tag{73}$$

Equation (73) gives the intensity pattern at each wavelength versus the spatial frequency. This pattern must be analyzed versus wavelength, what is done in Fig. 14 for the depolarizing device of Figs. 10 and 11(a). In this Fig. 14 all curves are normalized to their maximum values (versus spatial frequency) since we are here only interested in the beam alteration. Hence we work with the pattern:

$$R'(\lambda, \nu) = R(\lambda, \nu)/R_{max}(\lambda, \nu) \tag{74}$$

The left Fig. 14 is given for a reference and corresponds to the case where the reflected beam is not altered; hence this reference is calculated with a constant reflection factor yielding to classical Cardinal Sinus diffraction pattern, that is:

$$R'_{ref}(\lambda, \nu) = |sinc(\pi \nu L)|^2 \tag{75}$$

This reference is achromatic and exhibits the same sinc pattern at all wavelengths. It has to be compared to the other patterns given in the right Fig. 14, calculated for the depolarizing device for TE light polarized incident beam. As can be seen on the right figure, the reflected beam can be shifted or altered depending on the working wavelength. Fig. 15 is given for TM polarization and shows greater diffraction effects on the reflected beam. These effects result from the phase dispersion already shown in Fig. 11(b), which are not linear above the whole illumination area.

However since a pure beam deviation is not prohibitive for the application, a complete analysis requires to center all beams and replot these curves. The result is shown in Fig. 16 and emphasizes lower diffraction effects.

Optics EXPRESS

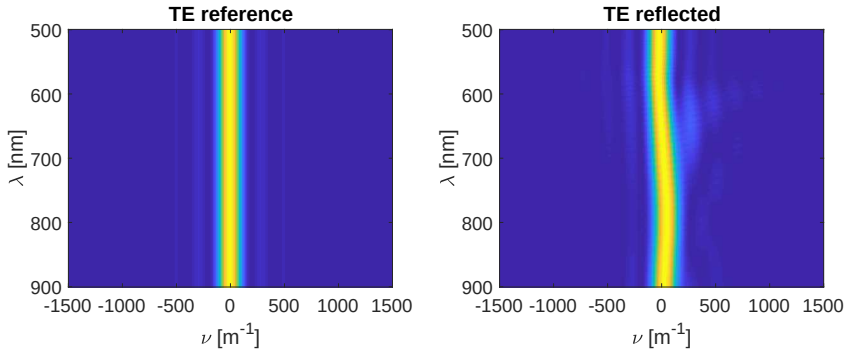

Fig. 14. TE reflected beam versus wavelength and spatial frequency. The left figure is the reference (see text) and the right figure emphasizes additional diffraction effects.

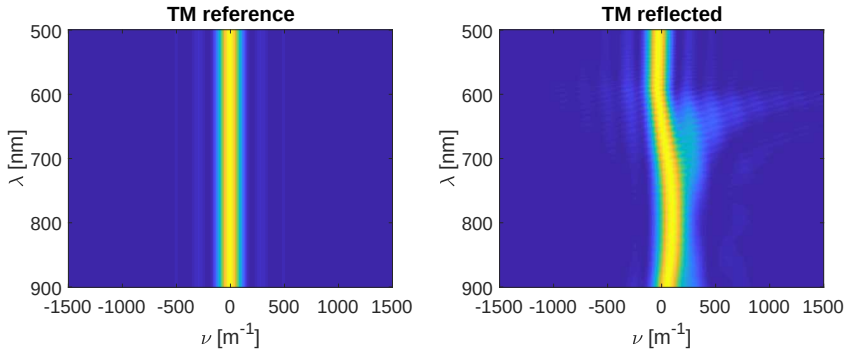

Fig. 15. TM reflected beam versus wavelength and spatial frequency. The left figure is the reference (see text) and the right figure emphasizes additional diffraction effects.

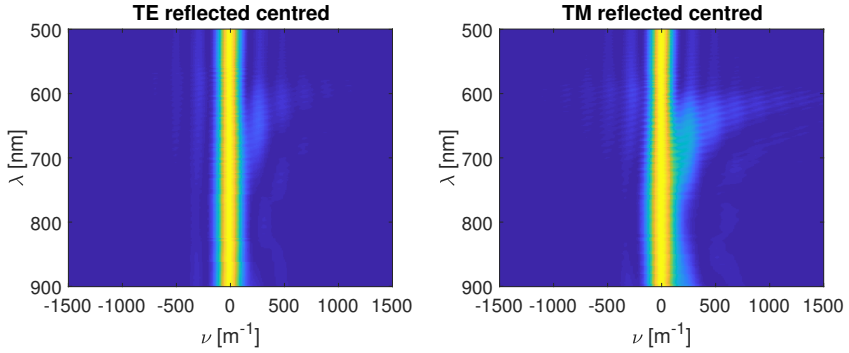

Fig. 16. TE and TM reflected beams after re-centering, for comparison to Fig. 15 (see text).

More detail about the alteration of the reflected beam is given in Fig. 17. For that we considered different sections of Fig. 16 at a constant wavelength. One section is given for the reference which gives a Cardinal Sinus. Another section is given at a wavelength with a negligible beam alteration ($\lambda_1 = 500nm$), and is quasi-superimposed to the reference. A last section is plotted in dashed line and is given to emphasize a noticeable beam deformation at wavelength $\lambda_2 = 633nm$.

To be complete, it is interesting to quantify the amount of energy which has spread outside the frequency width $\Delta\nu_{ref}$ of the reference. For that we considered the normalized curves which

Optics EXPRESS

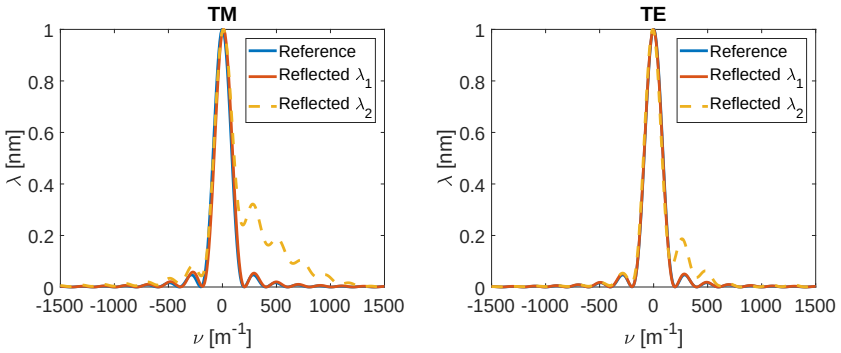

Fig. 17. Detail of beam alteration at two wavelengths $\lambda_1 = 500nm$ and $\lambda_2 = 633nm$ (see text). The λ_1 pattern is quasi-superimposed to the reference, while noticeable differences can be seen for the λ_2 pattern plotted in dashed line. The left and right figures are given for TM and TE polarization respectively.

have been centered, that is:

$$R''(\lambda, \nu) = R'(\lambda, \nu - \nu_0(\lambda)) \tag{76}$$

and we integrated them over the frequency range $\Delta\nu_{ref}$ of the reference:

$$F(\lambda) = \int_{\nu} R''(\lambda, \nu) d\nu \tag{77}$$

In a last step we normalize this quantify to that of the reference:

$$\eta(\lambda) = F(\lambda)/F_{ref}(\lambda) \tag{78}$$

The result is plotted in Fig. 18. The left figure is calculated with a bandwidth frequency of $1/L$, and the right figure with $3/L$. The reference is achromatic and close to 10% on the left figure, and to 2.7% on the right figure. We observe in the left figure that departures from the reference mainly occur in the depolarization band-pass ($600nm - 700nm$) and can reach 70% for TM polarization; the reason is that in this depolarization band, phase variations are required to cancel the mutual coherence, a condition required to depolarize light (see previous sections). Notice however that this is not a problem since these effects are strongly reduced in the right figure calculated with a bandwidth of $3/L$; actually receiver areas may easily collect greater solid angles.

7. Comparison to the bulk device

7.1. Depolarization

Thick anisotropic substrates have formerly provided solutions to depolarize light [21, 37–43]. The technique consists in using a bulk material with a similar cutting edge κ (see Fig. 19), so that the anisotropic optical paths create the depolarization. Such devices are necessarily used in transmission. Hence reflection must be here replaced by the transmission factors given for each polarization at normal incidence by:

$$t_{pol}(x) = t_{0,pol} exp[j(2\pi/\lambda) n_{pol} e_0] exp[j(2\pi/\lambda) n_{pol} x tan(\kappa')] \tag{79}$$

where $e = e_0 + x tan(\kappa')$ describes the substrate thickness variation, and n_{pol} is given for the polarization-dependent refractive index. Hence the polarimetric phase exhibits spatial linear variations given by:

Optics EXPRESS

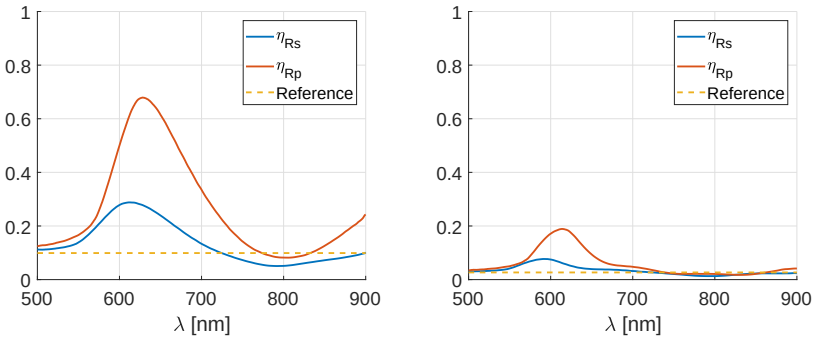

Fig. 18. Ratio versus wavelength of reflected energy from the depolarizing device and from the reference. The frequency range of integration is $1/L$ in the left figure and $3/L$ in the right figure.

$$\Delta\delta(x) = (2\pi/\lambda)\Delta n \ \ tan(\kappa')x = \gamma' x \tag{80}$$

with Δn the difference between the two indices. The slight losses at the interfaces are taken into account by $t_{0,pol}$ in Eq. (79), a Fresnel coefficient whose wavelength and polarization variations can be neglected for this application. Therefore Eq. (36) can be used and this leads to a spatial DOP given by:

$$DOP = |sinc(\gamma' L/2)| \qquad with \qquad \gamma' = (2\pi/\lambda)\Delta n \ \ tan(\kappa') \tag{81}$$

If we consider that the sinc function is zero above π, the depolarization condition can be written as:

$$\Delta n \ \ tan(\kappa') > \lambda/L \tag{82}$$

which is an easy condition to satisfy, that is, the greater the anisotropy the lower the cutting edge. Equation (81) allows a direct comparison of the performances of isotropic multilayers and anisotropic substrates. This comparison could be given by the phase slope denoted γ' for the bulk substrate and γ for the multilayer device, with the ratio $\gamma'/\gamma \approx 3\Delta n \ \ tan(\kappa')$. However this ratio is not a meaningful parameter for two reasons: first a minimum slope is enough to reach a total depolarization, that is, $\gamma > 2\pi/L \ \ or \ \ \gamma' > 2\pi/L$, both conditions which can be easily satisfied for the multilayer device and the bulk device respectively; and secondly a linear variation is not necessary to cancel the DOP with a gradient mirror, as said before. We conclude that the two devices have similar depolarization performances. The bulk anisotropic device works by transmission at low illumination angles, while the multilayer device works by reflection at oblique incidence. However the multilayer device provides a number of advantages. The first relies on its slight thickness, so that it can be integrated in microsystems; the second relies on the control of the depolarization band-pass (wide or narrow with a specific wavelength positioning), depending on the application.

7.2. Diffraction effect

As was done for depolarization in Section 5.3, we here consider the diffraction resulting from a depolarizing anisotropic substrate. Following Eq. (14), the Fourier transform of the transmitted field follows for each polarization:

$$\widehat{E}_t(\lambda, \nu, z) = A_0^+ \widehat{t}_{pol}(\lambda, \nu - \nu_0) e^{j\alpha(\lambda,\nu)z} \tag{83}$$

Optics EXPRESS

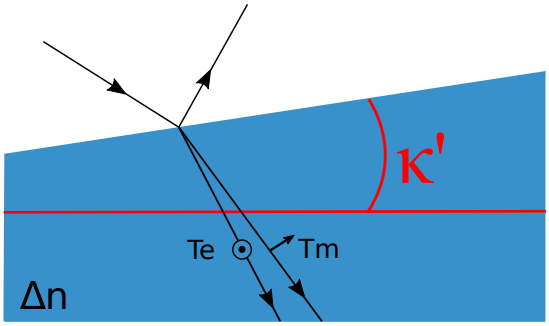

Fig. 19. Case of a birefringent substrate.

with

$$t_{pol}(x) = t_{0,pol} exp[j(2\pi/\lambda) n_{pol} e_0] exp[j(2\pi/\lambda) n_{pol} x tan(\kappa)] \tag{84}$$

where all parameters were previously defined for depolarization. Since the phase is here linear as:

$$\delta_{pol} = (2\pi/\lambda) n_{pol} tan(\kappa') x = 2\pi \gamma_{pol} x \tag{85}$$

with

$$\gamma = n_{pol} tan(\kappa')/\lambda \tag{86}$$

The Fourier Transform of transmission yields a single frequency deviation given by $\gamma_{pol}(\lambda)$, that is:

$$t_{pol}(\lambda, \nu - \nu_0) = t_{0,pol} exp[j(2\pi/\lambda) n_{pol} e_0] \delta[\nu - \nu_0 - \gamma_{pol}(\lambda)] \tag{87}$$

Hence there is no diffraction for the bulk depolarizer resulting from these linear phase variations, but only a beam shift. This deviation can be coupled to the depolarization condition Eq. (82), which yields to a minimum deviation:

$$(2\pi/\lambda) n_{pol} tan(\kappa') > n_{pol}/(L\Delta n) = \gamma_{min} \tag{88}$$

An order of magnitude can be calculated as follows:

$$\nu - \gamma_{min} = sin\theta/\lambda - \gamma_{min} = sin\theta'/\lambda \Rightarrow sin\theta - sin\theta' \approx \Delta\theta = \lambda\gamma_{min} = (\lambda/L)(n/\Delta n) \approx 10^{-4}/\Delta n \tag{89}$$

so it can be neglected for a moderate beam propagation distance. To conclude this section, diffraction does not occur for depolarizing bulk substrates, while it can be seen for multilayer devices. However this slight diffraction effect can be easily overcome if the solid angle is not limited to the minimum diffraction width $(1/L)$ of the reference, as discussed in Section 6. Notice also that the slight diffraction from the multilayer device must be considered in regard to the anisotropic refraction of the bulk substrate.

8. Conclusion

We have proposed optical multilayers as new devices to depolarize light without losses through a spatial process. These optical coatings exhibit polarimetric phase variations of reflection in their plane, and these variations are at the origins of the spatial depolarization. Such coatings can be produced with classical thin film deposition techniques if one takes advantage of non-uniformity

Optics EXPRESS

effects. Otherwise random phase variations can also be produced with photosensitive devices under speckle illumination. Taking advantage of uniformity effects, the depolarization procedure was shown to perfectly work when the incident wave is fully polarized with identical energy on each polarization mode ($\beta_0 = 1$). The thin film device then consists in a first classical (flat) mirror deposited on a substrate, which is over-layered with a gradient mirror. Such design allows to cancel losses ($\beta = 1$) in a controlled bandwidth, while it guarantees polarimetric phase variations able to cancel the mutual coherence in the same bandwidth. The result is a zero spatial DOP value in a large wavelength range, in phase opposition with the reflection coefficient. It was also shown how the procedure could be extended to depolarize light in a narrow bandwidth. We also checked that diffraction effects do not limit the application within the depolarization bandwidth. All results were shown to have performances similar to those of bulk anisotropic substrates which work by transmission. Hence the thin film devices act as efficient loss-less depolarizers with the advantage that they can be integrated in micro-optical systems. Furthermore, it was shown how the procedure can be extended to control arbitrary (narrow or broad-band) depolarizing bandwidths. Future work will concern experiment.

Funding

Centre National d'Etudes Spatiales (501100002830); Région Provence Alpes Côte d'Azur

Acknowledgments

This research was supported by the Centre National d'Etudes Spatiales (CNES) and by the Provence-Alpes-Cote-d'Azur (PACA) region.